Nanocomposite Catalysts

DOI: 10.1002/anie.200803968

Core–Satellite Nanocomposite Catalysts Protected by a Porous Silica Shell: Controllable Reactivity, High Stability, and Magnetic Recyclability**

*Jianping Ge, Qiao Zhang, Tierui Zhang, and Yadong Yin**

The development of more efficient and stable catalysts has been an increasingly important goal for chemists and materials scientists for both economic and environmental reasons. Much attention has been paid recently to nanoparticles of transition metals, particularly noble metals, as a result of significant progress in synthetic methods for controlling their composition, size, and shape. This development should lead to the design of catalysts with superior performance that take advantage of nanoparticles' high surface-to-volume ratio and their shape-dependent surface structure.[1–6] However, because of their high surface energies, nanoparticles tend to coagulate and/or change shape in catalytic reactions, and they eventually lose their initial activity and selectivity.[5–12] Therefore, it remains an important challenge to improve the stability, recyclability, and catalytic selectivity of metal nanocatalysts.

It has recently been realized that metallic nanoparticles can be greatly stabilized against coalescence by encapsulation within inorganic layers.[13–16] Unfortunately, dense inorganic coatings make it difficult for reactant molecules to reach buried active materials, limiting the use of this approach in catalysis. Encapsulation within porous shells makes the metal nanoparticles catalytically active and at the same time keeps them stable even under harsh reaction conditions.[17–23] Typically, the synthesis of these structures involves multiple steps and sacrificial templates, likely rendering the catalysts too expensive for widespread industrial use. In addition, few methods have been reported for systematic control over the pore sizes of the shells, making it difficult to control the mass transfer of the reactants and products.

A worthwhile synthetic challenge, therefore, is to develop a general, facile, and scalable approach to fabricating nanocatalyst systems where catalyst nanoparticles are protected within porous shells. We describe herein a convenient "encapsulation and etching" strategy that may provide a solution. Figure 1 schematically outlines the procedure. A monolayer of the metal nanocatalyst is first immobilized on the surface of silica colloids by using coupling agents. The core–satellite structures are then coated with another layer of silica of the desired thickness to fix the position of metal nanoparticles. Finally, a "surface-protected etching" technique is applied to make the outer shell mesoporous, exposing the catalyst particles to outside chemical species.[24] To improve the recyclability, we also incorporate a superparamagnetic Fe_3O_4 core at the center of the initial silica colloids.[25,26] Although several steps are required, the overall synthesis is highly reproducible and scalable. The sol–gel and etching procedures can be carried out sequentially at room temperature with simple setups. In addition, the inclusion of magnetic components allows efficient separation and purification during the synthesis by application of external magnetic fields. In contrast to the template-based methods, the etching process directly transforms dense silica coatings

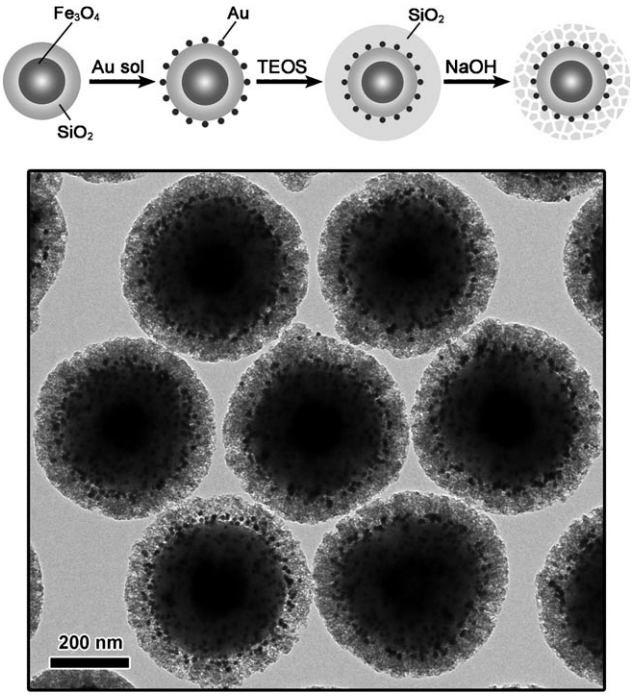

Figure 1. Synthetic procedure and a typical TEM image of porous silica protected Fe_3O_4/SiO_2/Au composite structures.

[*] Dr. J. Ge, Q. Zhang, Dr. T. Zhang, Prof. Y. Yin
Department of Chemistry, University of California
Riverside, CA 92521 (USA)
Fax: (+1) 951-827-4713
E-mail: yadong.yin@ucr.edu
Homepage: http://faculty.ucr.edu/~yadongy/

[**] Y. Yin thanks the University of California, Riverside for start-up funds. This research was supported by the Donors of the American Chemical Society Petroleum Research Fund. We also thank Prof. W. P. Beyermann and Dr. M. Biasini for help in measuring magnetic properties, and Prof. P. Feng, R. Liu, Prof. Y. Yan, and M. Sun for BET measurements.

Supporting information for this article is available on the WWW under http://dx.doi.org/10.1002/anie.200803968.

into porous shells; chemical species can reach the catalyst surface to participate in reactions but the shells still act as physical barriers preventing aggregation of the catalyst particles. Since nanoparticles with various sizes, shapes, and compositions can be loaded onto the silica surface through chemical coupling,[12,27,28] this process represents a general strategy for the synthesis of highly stable and readily recoverable nanocatalysts.

A typical synthesis starts with the preparation of highly responsive superparamagnetic cores of Fe_3O_4 by using a procedure reported previously.[25] After being coated with a layer of silica through a sol–gel process, the particle surfaces are further derivatized with a monolayer of the coupling agent 3-aminopropyltriethoxysilane (APTS) by heating the mixture in isopropanol at 80 °C. Citrate-stabilized Au nanoparticles are then able to adsorb onto the silica surface as the result of the strong chemical affinity between Au and primary amines. In the presence of polyvinylpyrrolidone (PVP), a second layer of silica is coated onto the composite colloid to fully encapsulate the Au nanoparticles within a silica matrix.[28,29] Mesoscale pores are then produced in the outer silica shell by first protecting the near surface layers of silica with PVP and subsequently etching with a highly concentrated aqueous NaOH solution. In this "surface-protected etching" process, refluxing the particles in water favors the penetration of PVP molecules in the silica surface by formation of strong hydrogen bonds between the carbonyl groups and the silanol groups.[30,31] The polymer chains with multiple binding groups can "cross-link" the SiO_2 subunits which dramatically increases the stability of the surface to NaOH etching. As a result, the NaOH solution diffuses through the silica surface and partially etches the unprotected silica, producing a mesoporous shell structure without changing the overall diameter of the composite particle. If etching is performed for only a relatively short period, the pore formation is mainly limited to the outer silica layer as the core silica is protected by adsorbed PVP. As shown in the transmission electron microscopy (TEM) image in Figure 1, the metal catalyst particles are sandwiched between the solid silica core and porous silica (por-SiO_2) shell. Such a configuration allows the catalyst particles to remain stable against coagulation while at the same time they are accessible to the reacting species outside of the shells.

The etching process can be well controlled by monitoring the transmittance of the colloidal solution. At extended etching times, more silica materials dissolve in the form of soluble silicate oligomers, and accordingly the transmittance increases. We have been able to precisely correlate the transmittance to the extent of etching. Figure 2 shows the TEM images of five samples collected after 50, 65, 85, 95, and 105 min of etching. Careful inspection of the TEM images indicates that the shells are rougher and less homogenous, suggesting the formation of porous structures. Thanks to the surface protection of PVP, the shell thickness shows no apparent change after moderate etching. Consistently, the transmittance of the solution increases from 29% to 45% with a near-linear dependence on the reaction time (Figure 2 f). Over-etching occurs after approximately 2 h when the silica shell becomes thinner, incomplete, and incapable of fully retaining the enclosed Au nanoparticles (see the Supporting Information).

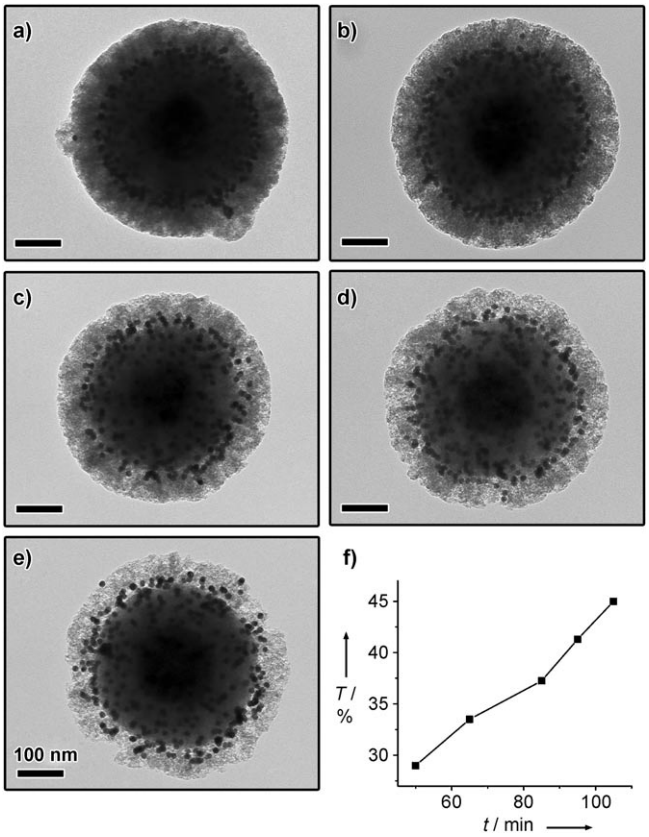

Figure 2. a–e) TEM images of $Fe_3O_4/SiO_2/Au/por\text{-}SiO_2$ composite colloids collected after different periods of etching: a) 50, b) 65, c) 85, d) 95, and e) 105 min. f) Changes in transmission intensity of the solution ($\lambda = 1000$ nm) as the silica shell is etched.

The average pore size increases upon etching. Figure 3 shows representative nitrogen adsorption/desorption isotherms and the corresponding pore size distribution of the sample displayed in Figure 2 b. The BET (Brunauer–Emmett–Teller) surface area and single-point total pore volume are 136.6 $m^2 g^{-1}$ and 0.25 $cm^3 g^{-1}$, respectively, which

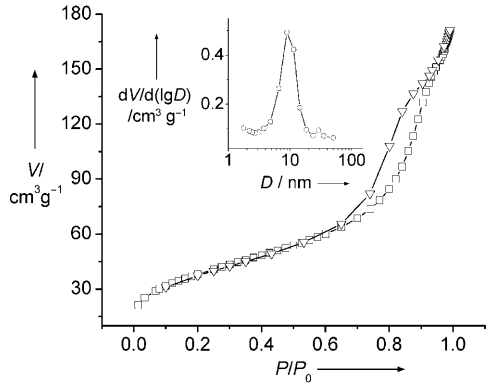

Figure 3. N_2 adsorption/desorption isotherms of the nanocomposite particles displayed in Figure 2 b. Inset shows the corresponding pore size distribution.

are considerably large values as the solid core and Au nanoparticles have been included in the calculations. The average BJH (Barret–Joyner–Halenda) pore diameter calculated from the desorption branch of the isotherm is determined to be 8.8 nm. For comparison, the BET surface area, total pore volume, and pore diameter of the sample displayed in Figure 2c have values of 112.8 $m^2 g^{-1}$, 0.27 $cm^3 g^{-1}$ and 13.2 nm, respectively (see the Supporting Information). The increase of pore size and volume with etching time is consistent with TEM observations of a gradual decrease in the transmission contrast of the shells.

Liquid-phase reduction of 4-nitrophenol (4-NP) by $NaBH_4$ was used as a model reaction to characterize the performance of the Au catalyst system.[23,32,33] Without the Au catalyst, the reduction does not proceed even with a large excess of $NaBH_4$. When a trace amount of our Fe_3O_4/SiO_2/Au/por-SiO_2 composite catalyst was introduced into the solution, the absorption at 400 nm decreased and absorption at 295 nm increased, indicating the reduction of 4-NP and formation of 4-aminophenol (4-AP), respectively. Since the concentration of $NaBH_4$ largely exceeds that of 4-NP ($C(NaBH_4)/C$(4-NP) = 333:1), the reduction can be considered as a pseudo-first-order reaction with regard to 4-NP only. Figure 4 shows

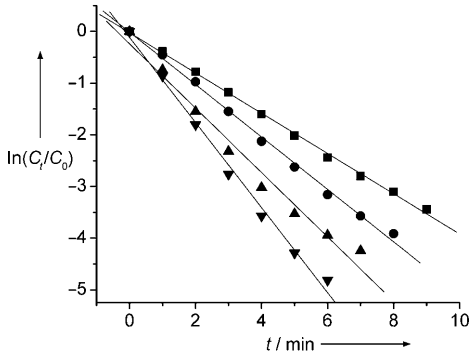

Figure 4. Relationship of $\ln(C_t/C_0)$ and reaction time t for the reduction of 4-NP catalyzed by the four composite catalysts shown in Figure 2; ■: catalyst corresponding to the Figure 2a; ●: Figure 2b; ▲: Figure 2c; ▼: Figure 2d. C_t and C_0 represent the concentration of 4-NP at time t and at the beginning of the reaction, respectively.

the linear relationship between $\ln(C_t/C_0)$ and reaction time t in reductions catalyzed by four catalyst systems with different degrees of etching (samples displayed in Figure 2a–d). As all these plots match the first-order reaction kinetics very well, the rate constant k can be calculated from the rate equation $\ln(C_0/C_t) = kt$ (Table 1). We also calculate the turnover frequency (TOF), which is defined as the number of moles of reduced 4-NP per mole surface Au atoms per hour when the conversion has reached 90%. Both the rate constant and TOF suggest higher catalytic efficiencies for Au nanocatalysts confined in shells with larger mesopores. The enhanced diffusion of reactants through the larger pores is believed to be responsible for the increased catalytic efficiency. The optical absorption and morphology of the catalysts remain almost unchanged after the catalytic reactions, demonstrating the superior stabilization effect of the porous shells. Although

Table 1: Comparison of kinetic constant (k) and turnover frequency (TOF) of 4-NP reduction using composite catalysts with different degrees of etching (samples displayed in Figure 2a–d).

Catalyst	k [min^{-1}]	TOF [h^{-1}]
a	0.39	617
b	0.51	799
c	0.62	1089
d	0.82	1363

larger pores are beneficial to the mass transfer, over-etching must be avoided as it will either produce pores that are too large to retain the Au particles, or make it difficult to completely isolate the neighboring Au particles from each other.

The magnetic properties of the composite structures have been investigated using a superconducting quantum interference device (SQUID) magnetometer prior to the recycling experiments. Figure 5a shows a hysteresis loop of typical composite colloids measured by sweeping the external field between −1 T and 1 T at room temperature. The Fe_3O_4 cores are approximately 140 nm in diameter. As expected, the magnetization curve shows no remanence or coercivity at room temperature, suggesting the superparamagnetic character essential for the magnetic separation and recycling as the particles are not subject to strong magnetic interactions in dispersion. The saturated mass magnetization is estimated to be 6.3 emu g^{-1}, which is consistent with the mass ratio (13 wt%) of Fe_3O_4 content in the composite colloid. As demonstrated in the photos in Figure 5a, the magnetic moment of the Fe_3O_4 core is sufficiently high that complete separation of catalyst colloids from the reaction solution can be achieved within 1–3 min in a relatively low magnetic field gradient (< 30 T m^{-1}).[25]

Although recyclability is usually regarded as an advantage of nanoparticle-based heterogeneous catalysts, their practical applications in liquid-phase reactions still suffer from both low efficiency of separation and reduced catalytic activity resulting from nanoparticle coagulation. The multilayer nanocomposite structures described here are designed to overcome these challenges. First, the catalysts can be recovered efficiently from the reaction solution by using external magnetic fields for many cycles without significant losses.[21,34] Second, the mesoporous SiO_2 framework can effectively stabilize the catalyst nanoparticles and prevent the reduction in activity due to coagulation, making the catalyst reusable after multiple cycles of reactions. Figure 5b and c compare the catalytic performance of Fe_3O_4/SiO_2/Au without and with the protection of a por-SiO_2 shell in six successive cycles of reactions, respectively. The concentration of $NaBH_4$ is decreased ($C(NaBH_4)/C$(4-NP) = 10:1) to slow down the reaction for convenient comparison of the conversion in the first 15 min of reactions. In the first cycle, the unprotected catalysts show high activity as all the Au nanocrystals immobilized on the core surface contribute to the catalysis without experiencing much resistance to mass transfer. However, catalytic reactions on the Au surface destabilize the Au–NH_2 interactions so that the particles gradually detach from the support surface and form large black aggregates with

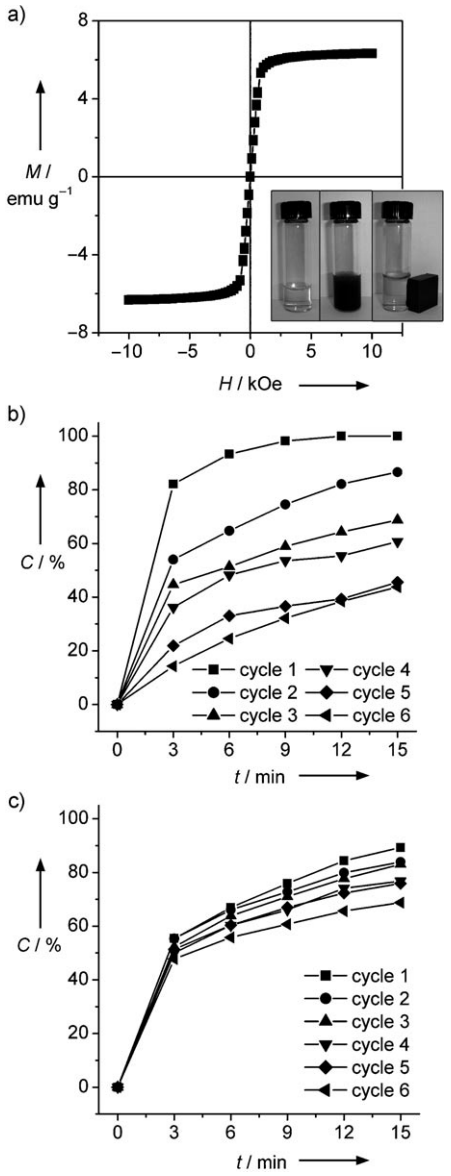

Figure 5. a) Mass magnetization *M* as a function of applied external field *H* for a typical composite catalyst at room temperature. The Fe_3O_4 cores have an average diameter of 140 nm. The photos in the inset demonstrate the convenient separation of the catalysts using an external magnetic field. b,c) Plot of conversion *C* of 4-NP as a function of reaction time *t* in six successive cycles of reduction and magnetic recycling using Fe_3O_4/SiO_2/Au core–satellite composite catalysts without (b) and with (c) the protection from the mesoporous silica shell.

dramatically reduced active surface areas (see the Supporting Information). As a result, the conversion ratio drops rapidly in the following cycles of reactions. On the other hand, the Au catalyst protected by por-SiO_2 maintains its activity well in the six successive cycles. The conversion of 4-NP drops only slightly primarily because small portions of the solution are removed for sampling (3.6% each cycle). Although the initial catalytic efficiency is slightly lower than that of the unprotected Au catalyst, the por-SiO_2-protected catalyst is much more durable in the following cycles of reactions. After the reactions, the Au catalysts protected by the por-SiO_2 shell remain dispersed on the core surface (see the Supporting Information). In this particular case, the relatively high concentration of $NaBH_4$ slowly etches the silica shell and slightly increases the pore size, which can be noticed in TEM measurement for samples after many cycles of reactions.

The "encapsulation and etching" strategy is a versatile approach for supporting and protecting nanoparticle catalysts with various sizes, shapes, and compositions.[12,27,28] As a further demonstration, we have incorporated Au nanoparticles 5 nm in diameter into the composite catalyst by using this procedure (see the Supporting Information). In addition, the composite catalyst described here has a number of advantages over the traditional metal nanocatalysts supported by the ordered mesoporous silica.[9,35–37] In the latter case, it is still a challenge to achieve uniform impregnation of the catalyst particles into the mesoporous channels with a reasonably high loading, and to minimize mass transfer resistance, particularly for porous structures with extended channel lengths. For our nanocomposite system, the thickness of the por-SiO_2 shells can be controlled even below 50 nm, which allows fast mass transfer of reagents to the embedded catalysts. Unlike the ordered mesoporous silica where catalyst can still grow as a result of particle migration within the channels,[9] our etched por-SiO_2 physically isolates the catalyst particles and prevents them from coming together during reactions.

In summary, mesoporous-silica-protected core–satellite nanocomposite catalysts have been fabricated through a series of simple sol–gel and surface-protected etching processes. These colloidal structures are ideal recyclable catalysts for liquid-phase reactions because they contain superparamagnetic components for efficient magnetic separation and a mesoporous silica framework for stabilization of the encapsulated catalyst particles. Such composite catalysts are expected to find use in industrial applications, where separation and recycling are critically required to reduce the cost as well as waste production. Although demonstrated with spherical silica cores, the procedure can also be extended to core materials with other shapes. More importantly, colloidal particles of many other metal oxides such as TiO_2, ZrO_2, SnO_2, and CeO_2 can be employed as the core material to support metal catalysts so that one can take advantage of the synergetic effects associated with specific metal oxide interfaces.[38–42]

Received: August 11, 2008
Published online: October 16, 2008

Keywords: gold · mesoporous materials · nanostructures · sol–gel processes · supported catalysts

[1] K. R. Gopidas, J. K. Whitesell, M. A. Fox, *Nano Lett.* **2003**, *3*, 1757.
[2] L. K. Yeung, R. M. Crooks, *Nano Lett.* **2001**, *1*, 14.
[3] R. Narayanan, M. A. El-Sayed, *J. Am. Chem. Soc.* **2003**, *125*, 8340.
[4] G. A. Somorjai, *Appl. Surf. Sci.* **1997**, *121/122*, 1.
[5] Y. Li, J. Petroski, M. A. El-Sayed, *J. Phys. Chem. B* **2000**, *104*, 10956.

[6] R. Narayanan, M. A. El-Sayed, *J. Am. Chem. Soc.* **2004**, *126*, 7194.
[7] G. Budroni, A. Corma, *Angew. Chem.* **2006**, *118*, 3406; *Angew. Chem. Int. Ed.* **2006**, *45*, 3328.
[8] W. Yan, S. Mahurin, S. Overbury, S. Dai, *Top. Catal.* **2006**, *39*, 199.
[9] R. M. Rioux, H. Song, J. D. Hoefelmeyer, P. Yang, G. A. Somorjai, *J. Phys. Chem. B* **2005**, *109*, 2192.
[10] R. Narayanan, M. A. El-Sayed, *J. Phys. Chem. B* **2005**, *109*, 12663.
[11] M. Comotti, C. D. Pina, R. Matarrese, M. Rossi, *Angew. Chem.* **2004**, *116*, 5936; *Angew. Chem. Int. Ed.* **2004**, *43*, 5812.
[12] I. Pastoriza-Santos, D. Gomez, J. Pérez-Juste, L. M. Liz-Marzán, P. Mulvaney, *Phys. Chem. Chem. Phys.* **2004**, *6*, 5056.
[13] M. Ohmori, E. Matijevic, *J. Colloid Interface Sci.* **1992**, *150*, 594.
[14] A. P. Philipse, M. P. B. van Bruggen, C. Pathmamanoharan, *Langmuir* **1994**, *10*, 92.
[15] L. M. Liz-Marzan, M. Giersig, P. Mulvaney, *Langmuir* **1996**, *12*, 4329.
[16] Y. Lu, Y. Yin, Z. Y. Li, Y. Xia, *Nano Lett.* **2002**, *2*, 785.
[17] H. J. Hah, J. I. Um, S. H. Han, S. M. Koo, *Chem. Commun.* **2004**, 1012.
[18] J. Y. Kim, S. B. Yoon, J.-S. Yu, *Chem. Commun.* **2003**, 790.
[19] M. Kim, K. Sohn, H. B. Na, T. Hyeon, *Nano Lett.* **2002**, *2*, 1383.
[20] S. Ikeda, S. Ishino, T. Harada, N. Okamoto, T. Sakata, H. Mori, S. Kuwabata, T. Torimoto, M. Matsumura, *Angew. Chem.* **2006**, *118*, 7221; *Angew. Chem. Int. Ed.* **2006**, *45*, 7063.
[21] Y. L. Shi, T. Asefa, *Langmuir* **2007**, *23*, 9455.
[22] M. Shokouhimehr, Y. Piao, J. Kim, Y. Jang, T. Hyeon, *Angew. Chem.* **2007**, *119*, 7169; *Angew. Chem. Int. Ed.* **2007**, *46*, 7039.
[23] J. Lee, J. C. Park, H. Song, *Adv. Mater.* **2008**, *20*, 1523.
[24] Y. Hu, J. Ge, Y. Sun, T. Zhang, Y. Yin, *Nano Lett.* **2007**, *7*, 1832.
[25] J. Ge, Y. Hu, M. Biasini, W. P. Beyermann, Y. Yin, *Angew. Chem.* **2007**, *119*, 4420; *Angew. Chem. Int. Ed.* **2007**, *46*, 4342.
[26] J. Ge, T. Huynh, Y. Hu, Y. Yin, *Nano Lett.* **2008**, *8*, 931.
[27] J. Kim, J. E. Lee, J. Lee, Y. Jang, S.-W. Kim, K. An, J. H. Yu, T. Hyeon, *Angew. Chem.* **2006**, *118*, 4907; *Angew. Chem. Int. Ed.* **2006**, *45*, 4789.
[28] C. Graf, S. Dembski, A. Hofmann, E. Ruhl, *Langmuir* **2006**, *22*, 5604.
[29] C. Graf, D. L. J. Vossen, A. Imhof, A. vanBlaaderen, *Langmuir* **2003**, *19*, 6693.
[30] M. A. Cohen Stuart, G. J. Fleer, B. H. Bijsterbosch, *J. Colloid Interface Sci.* **1982**, *90*, 321.
[31] V. M. Gun'ko, V. I. Zarko, E. F. Voronin, E. V. Goncharuk, L. S. Andriyko, N. V. Guzenko, L. V. Nosach, W. Janusz, *J. Colloid Interface Sci.* **2006**, *300*, 20.
[32] S. Panigrahi, S. Basu, S. Praharaj, S. Pande, S. Jana, A. Pal, S. K. Ghosh, T. Pal, *J. Phys. Chem. C* **2007**, *111*, 4596.
[33] Y. Lu, Y. Mei, M. Drechsler, M. Ballauff, *Angew. Chem.* **2006**, *118*, 827; *Angew. Chem. Int. Ed.* **2006**, *45*, 813.
[34] Y. Deng, D. Qi, C. Deng, X. Zhang, D. Zhao, *J. Am. Chem. Soc.* **2008**, *130*, 28.
[35] J. Zhu, Z. Konya, V. F. Puntes, I. Kiricsi, C. X. Miao, J. W. Ager, A. P. Alivisatos, G. A. Somorjai, *Langmuir* **2003**, *19*, 4396.
[36] H. Zhu, Z. Ma, S. Overbury, S. Dai, *Catal. Lett.* **2007**, *116*, 128.
[37] M. T. Bore, M. P. Mokhonoana, T. L. Ward, N. J. Coville, A. K. Datye, *Microporous Mesoporous Mater.* **2006**, *95*, 118.
[38] M. Haruta, *Catal. Today* **1997**, *36*, 153.
[39] M. Valden, X. Lai, D. W. Goodman, *Science* **1998**, *281*, 1647.
[40] J.-D. Grunwaldt, M. Maciejewski, O. S. Becker, P. Fabrizioli, A. Baiker, *J. Catal.* **1999**, *186*, 458.
[41] M. M. Schubert, S. Hackenberg, A. C. van Veen, M. Muhler, V. Plzak, R. J. Behm, *J. Catal.* **2001**, *197*, 113.
[42] A. Corma, P. Serna, *Science* **2006**, *313*, 332.

